Modeling Laser Intensities For Simultaneous Localization and Mapping

Sheraz Khan, *Student Member, IEEE*, Dirk Wollherr, *Senior Member, IEEE*, and Martin Buss, *Fellow, IEEE*

***Abstract*—The objective of this letter is to develop a data-driven model of laser intensities and investigate its usage for simultaneous localization and mapping (SLAM) in the field of robotics. In contrast to the standard usage of laser scanners in SLAM to generate geometric models of the environment, the research work on the applications of laser intensities is rather limited. A typical laser scanner measures the distance to an object as well as quantifies the received optical power after reflection which is termed as *intensity*. The most interesting and relevant aspect of intensities in context of this letter is that they are dependent on an intrinsic surface property i.e., reflectivity as well as extrinsic parameters such as the distance to the surface and angle of incidence with respect to the surface normal. This letter focuses on modeling the influence of extrinsic parameters on intensities to acquire a pose-invariant measure of surface reflectivity. This measure is used in an extension of Hector SLAM in which a robot simultaneously acquires a geometric model augmented with surface reflectivity characteristics. An extensive experimental evaluation is carried out in an indoor environment to highlight the advantages and characteristics of the data-driven model and the proposed Hector SLAM extension.**

***Index Terms*—SLAM, mapping, laser intensities, surface reflectivity, Hector SLAM.**

I. Introduction

THE RESEARCH work in the field of SLAM [1]–[3] has provided autonomous robots the capability of simultaneously estimating their own pose as well as acquiring an accurate topologic/metric map of the environment. The majority of the research work in the domain of laser based SLAM focuses on generating an accurate geometric model of the environment. In addition to measuring the distance to an object, a typical laser scanner also quantifies the remission values, i.e. received optical power, after reflection from the surface. This remission value is termed as *intensity* and depends (among other parameters) on an intrinsic surface property (surface reflectivity) as well as extrinsic parameters such as distance to the surface and angle of incidence. *The basic idea is to model the influence of the extrinsic parameters to acquire a pose-invariant measure of surface reflectivity which can serve as additional information in a variety of robotic applications*. Hence, the objective of this letter is to develop a *simple data-driven model* of laser intensities to acquire a pose-invariant measure of surface reflectivity. In addition, an extension of Hector SLAM [1] is presented which is capable of generating a *reflectivity map (occupancy grid augmented with surface reflectivity characteristics)*. It is important to highlight the scope of the proposed approach within the SLAM framework. In graph SLAM a distinction is made between the SLAM front-end and the back-end. The front-end deals with the raw sensor data to generate nodes and edge constraints whereas the back-end estimates the posterior distribution of the robot poses given all edge constraints. The proposed approach (see Section IV) serves as a component of the SLAM front-end which estimate the transformation (using surface reflectivities) between robot poses (edge constraints) and furthermore acquires a reflectivity map. In principle, any graph SLAM back-end [3]–[5] can be coupled with the proposed approach as SLAM back-ends are considered to be sensor agnostic using the notion of *virtual measurements* [4]. The capability of generating a geometric model augmented with surface reflectivity characteristics provides the possibility of using this information to enhance the performance of SLAM, global localization [6] or loop closure [7], [8] algorithms in specific scenarios. To explain this briefly in the context of pose estimation for SLAM, consider a corridor scene in which a robot observes two parallel flat walls composed of different surfaces, each having different reflectivity characteristics. In such a scenario, the robot pose estimate along the principal direction of the corridor is degenerate if only metric information is used (assuming bad odometry estimates). In contrast, the usage of surface reflectivities could lead to accurate pose estimates due to the presence of additional features. The emphasis of this letter is on the development of a *data-driven model* of intensities and its usage in the *SLAM front-end* in *indoor* environments. The evaluation of the proposed data-driven model in outdoor environments as well as the application of laser intensities in the context of loop closure and global localization is beyond the scope of this letter and thereby left as future work.

Manuscript received August 30, 2015; accepted December 17, 2015. Date of publication January 12, 2016; date of current version February 29, 2016. This paper was recommended for publication by Associate Editor J. Nieto and Editor C. Stachniss upon evaluation of the reviewers' comments. This work was supported by the ERC Advanced Grant SHRINE Agreement no. 267877.

S. Khan and M. Buss are with the Chair of Automatic Control Engineering, Technische Universität München, 80333 Munich, Germany, and also with the TUM Institute for Advanced Study, Technische Universität München, Garching 85748, Germany (e-mail: sheraz.khan@tum.de; mb@tum.de).

D. Wollherr is with the Chair of Automatic Control Engineering, Technische Universität München, 80333 Munich, Germany (e-mail: dw@tum.de).

Digital Object Identifier 10.1109/LRA.2016.2516592

II. Related Work and Contribution

In the last few decades a large amount of research work has been carried out in the field of SLAM [1]–[3], [5] in which a robot generates a geometric model of its environment based on observations from a laser scanner. In contrast, the research work on the applications of laser intensities in the domain of SLAM and to a certain extent in the field of robotics is rather insignificant. In [11], the authors use retro-reflective markers as artificial beacons due to significant difference in their surface reflectivity to identify landmarks for SLAM. The most relevant

research work with respect to this letter is presented in [12] in which an iterative closest point (ICP) [13] variant is presented that uses intensities to determine point correspondences between consecutive scans for transformation estimation. The above mentioned approach assumes that the robot pose does not change significantly thereby ignoring the influence of extrinsic parameters. In contrast, this letter focuses on developing a *data-driven* approach to model the influence of extrinsic parameters on laser intensities to acquire a pose-invariant measure of surface reflectivity. These reflectivity characteristics are stored in a *reflectivity map* for which the pose-invariance property is important as the same surface might be observed by the robot from different poses. In addition, the reflectivity characteristics are also used for pose estimation by matching the current scan (equipped with intensities) with an already acquired reflectivity map during which the robot pose can change significantly (depending on the map update rate). In contrast to the field of SLAM, laser intensities have been used for human detection [14], localization [15], visual odometry [16], terrain classification [17] and object tracking [18], [19]. The main contributions of this letter are highlighted below:

- A *simple data-driven* approach to model laser intensities for different scanners (Section III-B)
- An extension of Hector SLAM capable of acquiring geometric models augmented with surface reflectivity characteristics (Section IV)
- An evaluation of the proposed *data-driven* approach and Hector SLAM extension (Section V)

III. Modeling Laser Intensities

This section is divided into two main subsections. The first subsection focuses on the motivation for developing a *data-driven* approach to model laser intensities whereas the second subsection discusses the details of this data-driven approach.

A. Motivation for a Data-Driven Approach

This letter discusses the intensity characteristics of the most commonly used scanners in the field of robotics namely Hokuyo UTM-30LX and SICK LMS 291-S05[1]. To identify the extrinsic parameters which influence the intensity characteristics it is essential to consider the LIDAR equation which is commonly used in the field of remote sensing [20], [21]. The LIDAR equation given the lambertian reflector assumption defines the relation between the received optical power P_{rec} and extrinsic parameters

$$I_{\text{rec}} \propto P_{\text{rec}} \propto \frac{\varrho \cos(\alpha)}{r^2}, \tag{1}$$

where ϱ represents the surface reflectivity, r represents the distance (radial coordinate/distance) to the surface and α corresponds to the angle of incidence. The proportionality between P_{rec} and extrinsic parameters exists due to presence of additional contant parameters such as the emitted power P_{emit}, system transmission factors, aperture diameter etc. [9], [23]. I_{rec} represents the intensity increment, which is obtained after post-processing of the received optical power P_{rec} by the laser scanner. The intensity increment is assumed to be proportional to the received optical power. Eq. (1) defines the parameters which influence intensities, hence the distance r and the angle of incidence α are the extrinsic factors that need to be considered during the modeling phase. In contrast, ϱ is an intrinsic surface property; which is useful for differentiating surfaces with different reflectivity properties. Although (1) contains all the extrinsic parameters that influence intensities, it is a crude approximation and does not consistently (over the complete domain of distance and angle of incidence) explain the empirical data for high-end terrestrial scanners [9], [24] as well as the laser scanners investigated in this letter. To explain this briefly, consider the inverse square relationship in (1). Figure 1(a) and 1(b) shows the variation of the intensity increment I_{rec} for the Hokuyo and SICK scanner as a function of distance r (with a fixed angle of incidence $\alpha \approx 0°$) given the *same surface (fixed ϱ) i.e. standard white printing paper*. It can be seen that the inverse square distance relationship breaks down at close distances because I_{rec} starts decreasing instead of increasing. This effect has also been observed for high powered terrestrial laser scanners [9], [24] and has been termed the *near distance* effect. In photogrammetry and remote sensing literature this effect has been attributed to the defocusing of the receiver optics [9] (causing P_{rec} to decrease and consequently I_{rec} to decrease) for certain terrestrial laser scanners such as the Z+F[2] scanner. In principle, this effect is largely dependent on the intrinsic design and internal processing performed by the laser scanner (Riegl[3] scanners exhibit different intensity characteristics at near distances [24]), the details of which are not readily provided by companies making it difficult to ascribe a specific reason in case of the Hokuyo and SICK scanner. Similarly, in our evaluation the variation of normalized intensity as a function of α (after removal of the influence of r - see caption of Figure 1) also does not follow the $\cos(\alpha)$ model as shown in Figure 1(c) and 1(d). This inconsistency is generally attributed to the assumption that the surface should exhibit lambertian reflectance which is rarely the case. The highlighted inconsistency as well as the scarcity of system-based-models due to lack of information from laser companies about the internal processing and intrinsic design is the main motivation for developing a *data-driven* approach to model intensities. The objective of this model is to quantify the variation of intensity as a function of r and α to acquire a pose-invariant measure of surface reflectivity. Two different strategies can be adopted to develop a *simple data-driven* model, firstly assuming that the variation in intensity due to r and α can be modeled independently

$$I_{\text{rec}} \propto P_{\text{rec}} \propto \varrho f(r) f(\alpha), \tag{2}$$

where $f(r)$ and $f(\alpha)$ are the estimated data-driven functions defining the effect on intensities. In contrast, the second strategy is to develop a model as

$$I_{\text{rec}} \propto P_{\text{rec}} \propto \varrho f(r, \alpha), \tag{3}$$

where $f(r, \alpha)$ jointly models the variation in intensities due to r and α. Figure 1(c) and 1(d) helps in assessing the plausibility

[1]Intensities for the SICK LMS 291-S05 scanner were acquired by configuring the scanner to the undocumented measuring mode 13 (0Dh). The subcommand 2Bh can be used to request distance and reflectivities to which the scanner responds with the response F5h [22].

[2]http://www.zf-laser.com/

[3]http://www.riegl.com/

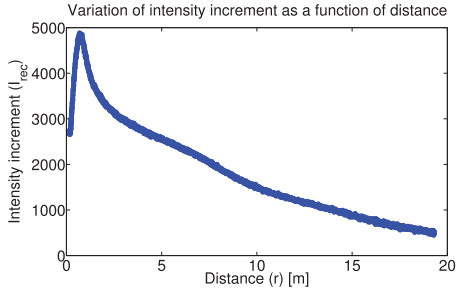

(a) Intensity increment I_{rec} as a function of the distance r (radial coordinate/distance) for the Hokuyo scanner

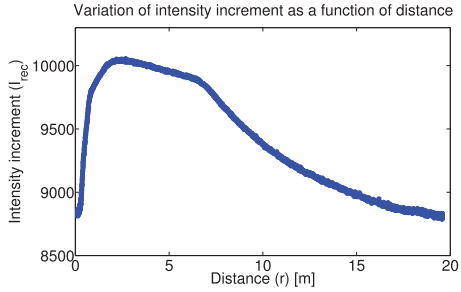

(b) Intensity increment I_{rec} as a function of distance r (radial coordinate/distance) for the SICK scanner

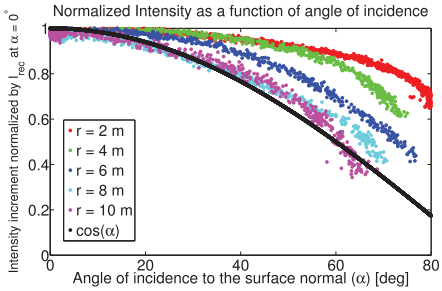

(c) Normalized intensity as a function of angle of incidence α for different fixed distances r in case of the Hokuyo scanner

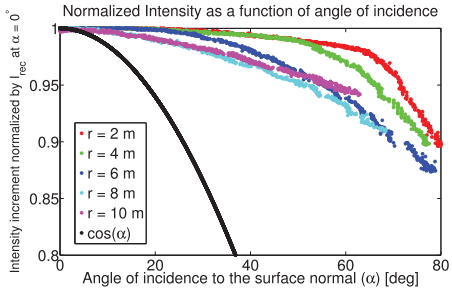

(d) Normalized intensity as a function of angle of incidence α for different fixed distances r in case of the SICK scanner

Fig. 1. Intensity characteristics of the Hokuyo UTM-30LX and the SICK LMS 291-S05 scanner as a function of distance r in meters (radial coordinate/distance) and angle of incidence α in degrees for standard white printing paper. a-b) The intensity characteristics of the Hokuyo and the SICK scanner as a function of distance r with a fixed angle of incidence with respect to the surface normal ($\alpha \approx 0°$). Both scanners exhibit a decrease in intensity increment I_{rec} at close distances which is termed the *near distance* effect [9]. The intensity characteristics are shown up to a distance of 19 meters as all experimental evaluations were carried out in indoor environments in this letter (18–20 m being the distance between the furthest surfaces). c-d) The variation in intensity as a function of α given that the surface is observed at a fixed distance r in case of the Hokuyo and SICK scanner. The influence of the distance r is removed by normalizing the intensity, i.e. dividing the intensity increment with the value corresponding to $\alpha = 0°$, for a fixed distance r. Hence, the normalized intensity lies in the [0 1] interval. It is important to highlight that the angle of incidence is calculated by taking the dot product between the laser beam direction and the surface normal. The surface normal is the eigenvector corresponding to the smallest eigenvalue of the covariance matrix which is estimated by considering the neighborhood around a certain point [10]. As the estimation of the surface normal degrades with point cloud density, the intensity characteristics could only be acquired up to $\alpha \leq 80°$ for small distances and $\alpha \leq 60°$ at large distances.

of the assumptions in (2) and (3). If the assumption in (2) is true, the variation in the normalized intensity (effectively the removal of the influence due to r) should be the same at different r, however Figure 1(c) and 1(d) shows that this assumption does not hold for the Hokuyo and the SICK scanner at $\alpha \geq 20°$ for different r. Given the trend in Figure 1(c) and 1(d), this letter focuses on a *data-driven* approach to model intensities using (3).

B. Proposed Approach

This section defines a simple *data-driven* approach to model laser intensities and acquire a measure of surface reflectivity. Given a material with a known reflectivity coefficient ϱ, it is possible to calibrate and determine the function $f(r, \alpha)$ in (3). In case of unavailability of a surface with known reflectivity it is possible to acquire a *relative measure of surface reflectivity*. In this letter the second option is considered due to its simplicity and applicability even in case of absence of standard materials with known reflectivity. Hence, the calibration process requires a *reference* surface (standard white printing paper) for which the intensities are measured as

$$I_{\text{ref}} \propto P_{\text{ref}} \propto \varrho_{\text{ref}} f(r, \alpha). \tag{4}$$

Eq. (3) defines the intensity increment I_{rec} for a specific surface with reflectivity ϱ being currently observed at a specific r and α whereas (4) defines the intensity increment I_{ref} for the reference surface at the same r and α. Hence, (3) and (4) can be used to acquire a *relative measure of surface reflectivity* as

$$\frac{I_{\text{rec}}}{I_{\text{ref}}} \propto \frac{P_{\text{rec}}}{P_{\text{ref}}} \propto \frac{\varrho f(r, \alpha)}{\varrho_{\text{ref}} f(r, \alpha)} = \frac{\varrho}{\varrho_{\text{ref}}} = \bar{\varrho}. \tag{5}$$

The relative measure $\bar{\varrho}$ defines the reflectivity of the measured surface with respect to the reference surface (white paper). *It is important to specify that this model assumes that the function $f(r, \alpha)$ varies in the same manner for all surfaces*, hence ignoring any coupling of the function f with ϱ. In the experimental evaluation carried out in indoor environments (see Section V) this assumption yielded good results. The proposed mechanism, of using the function $f(r, \alpha)$, is a data-driven formulation in contrast to the standard $\cos(\alpha)$ and inverse squared distance model. An important aspect of the proposed model is the approximation of I_{ref} which is proportional to $\varrho_{\text{ref}} f(r, \alpha)$. This approximation is performed by collecting observations of the reference surface at different r and α. Since it is not possible to acquire values at every r and α, a scattered interpolant (with linear interpolation) is used to approximate the values between

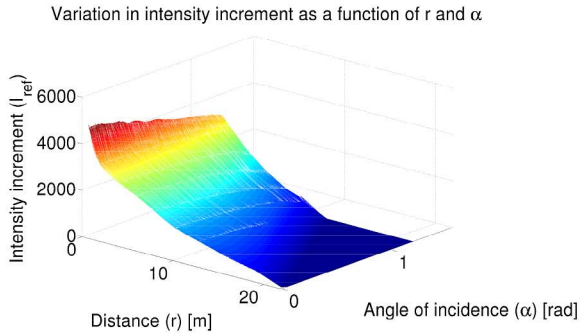

(a) Approximated intensity increment $I_{\text{ref}} \propto \varrho_{\text{ref}} f(r, \alpha)$ for Hokuyo UTM30-LX

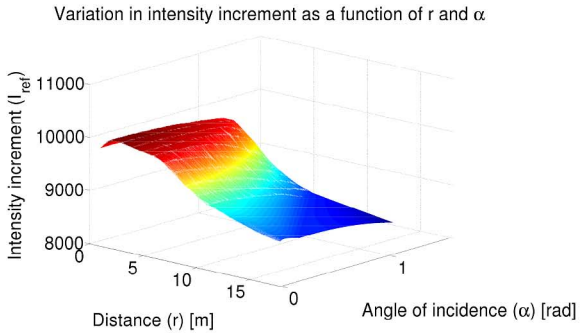

(b) Approximated intensity increment $I_{\text{ref}} \propto \varrho_{\text{ref}} f(r, \alpha)$ for SICK LMS 291-S05

Fig. 2. The approximated intensity increment $I_{\text{ref}} \propto \varrho_{\text{ref}} f(r, \alpha)$ surface of the Hokuyo and the SICK scanner. The intensity characteristics are acquired up to a distance of 18–20 m as all experimental evaluations were carried out in indoor environments (for indoor environments this calibration is sufficient). If required the proposed approach could be extended to acquire intensity characteristics over a wider r and α domain.

given observations. This approximated surface obtained for the Hokuyo and SICK scanner is shown in Figure 2. This surface is furthermore sampled using a *fine* grid over r and α to generate a *lookup table* (LUT) based model. The main advantage of this LUT based model is that it can be computed offline and during online operation it requires simple array indexing thereby reducing computational cost.

IV. Extension of Hector SLAM

This section focuses on using the relative reflectivity measure in an extension of Hector SLAM [1] in which a robot acquires a reflectivity map. The first subsection explains the grid structure whereas the second subsection focuses on the transformation estimation process based on the surface reflectivity measure by matching the current scan at time index t with an already acquired reflectivity map until time $t-1$.

A. Occupancy and Reflectivity Grid Structure

Let $G = \{g_1, \ldots, g_p\}$ represent the regular grid structure which stores two different attributes, firstly the occupancy probability $P(g_i)$ and the surface reflectivity measure $R(g_i)$ observed for the i^{th} grid cell g_i. Let $z_t = \{\{\mathbf{s}_1^t, \bar{\varrho}_1^t\}, \ldots \{\mathbf{s}_n^t, \bar{\varrho}_n^t\}\}$ be the observation of the scanner at time index t consisting of n cartesian coordinates and surface reflectivity measures (obtained from the LUT based model). The notation $\mathbf{s}_i^t = [s_{i,x}^t, s_{i,y}^t]$ corresponds to the world coordinate beam end points. The occupancy probability of a grid cell is calculated using the standard recursive occupancy update equation [25]–[27]

$$P(g_i|z_{1:t}) = \left[1 + \frac{1 - P(g_i|z_t)}{P(g_i|z_t)} \frac{1 - P(g_i|z_{1:t-1})}{P(g_i|z_{1:t-1})} \frac{P(g_i)}{1 - P(g_i)}\right]^{-1},$$

which is a commonly used inverse sensor model in robotic mapping. $P(g_i|z_{1:t})$ represents the occupancy probability of the i^{th} grid cell given all observations. $P(g_i)$ represents the occupancy probability of a grid cell prior to any observations. $P(g_i|z_t)$ and $P(g_i|z_{1:t-1})$ represent the probability given the most current sensor observation z_t and observations since the beginning of time until time $t-1$ respectively. The above mentioned equation can be converted to the log odds form to simplify the computation.

In addition to the occupancy probability, the grid structure also stores the relative reflectivity measure of the surface for the i^{th} cell g_i. In the ideal case the reflectivity measure would be invariant to the robot pose thereby yielding a constant value for a specific surface, however a violation of the assumption in Section III-B or inaccurate surface normal estimation can cause reflectivity characteristics to vary. In this letter the reflectivity measure of each grid cell is calculated using a simple incremental averaging mechanism

$$R_{\text{m}}(g_i|z_t) = R_{\text{m}}(g_i|z_{t-1}) + \frac{{}^i\bar{\varrho}_j^t - R_{\text{m}}(g_i|z_{t-1})}{n_{g_i}},$$

where $R_{\text{m}}(g_i|z_t)$ represents the incremental mean of all the surface reflectivity observations till time index t. ${}^i\bar{\varrho}_j^t$ represents the j^{th} reflectivity measure in the sensor observation z_t for the i^{th} grid cell g_i and n_{g_i} represents the total number of sensor observations for g_i. The left superscript of the reflectivity measure $\bar{\varrho}$ is not mentioned explicitly unless necessary for clarification.

Due to the discrete nature of the grid a bilinear interpolation scheme is adopted to allow subgrid accuracy as done in the original Hector SLAM paper [1]. However, the proposed approach interpolates the *relative surface reflectivity measure* rather than the occupancy probabilities and additionally frames the transformation estimation problem using this measure as discussed in the next subsection. Given a continuous coordinate P, the reflectivity value $R(P)$ is approximated by using the four closest grid cells coordinates (assuming the indices to be (i, j, k, l) with $x_i = x_k$, $x_j = x_l$, $y_i = y_j$ and $y_k = y_l$. x_*, y_* are the metric coordinates of cell g_* in the geometric map) as

$$\begin{aligned} R(P) \approx \frac{y - y_i}{y_k - y_i} \left(\frac{x - x_i}{x_j - x_i} R_{\text{m}}(g_l) + \frac{x_j - x}{x_j - x_i} R_{\text{m}}(g_k) \right) \\ + \frac{y_k - y}{y_k - y_i} \left(\frac{x - x_i}{x_j - x_i} R_{\text{m}}(g_j) + \frac{x_j - x}{x_j - x_i} R_{\text{m}}(g_i) \right). \end{aligned}$$

Similarly the gradient $\nabla R(P) = \left(\frac{\partial}{\partial x} R(P), \frac{\partial}{\partial y} R(P) \right)$ is approximated as in [1] by replacing the occupancy probabilities with the reflectivity measure

$$\frac{\partial R(P)}{\partial x} \approx \frac{y - y_i}{y_k - y_i}\left(R_{\mathrm{m}}(g_l) - R_{\mathrm{m}}(g_k)\right) + \frac{y_k - y}{y_k - y_i}\left(R_{\mathrm{m}}(g_j) - R_{\mathrm{m}}(g_i)\right),$$

$$\frac{\partial R(P)}{\partial y} \approx \frac{x - x_i}{x_j - x_i}\left(R_{\mathrm{m}}(g_l) - R_{\mathrm{m}}(g_j)\right) + \frac{x_j - x}{x_j - x_i}\left(R_{\mathrm{m}}(g_k) - R_{\mathrm{m}}(g_i)\right).$$

B. Scan Matching

This section explains the robot pose estimation process to align the new sensor observation with an existing reflectivity map. The proposed Hector SLAM extension formulates the estimation of the robot pose $\zeta = [t_x, t_y, \theta]$ as the minimization of the cost function

$$\zeta^* = \arg\min_{\zeta} \sum_{i=1}^{n} \left[\bar{\varrho}_i^t - R(\mathbf{S}_i(\zeta))\right]^2, \tag{6}$$

where $\bar{\varrho}_i^t$ represents the reflectivity measure of the i^{th} beam end point in the sensor observation z_t and $R(\mathbf{S}_i(\zeta))$ corresponds to the reflectivity measure in the map based on the transformed beam end point coordinates $\mathbf{S}_i(\zeta)$ as

$$\mathbf{S}_i(\zeta) = \begin{pmatrix} \cos(\theta) & -\sin(\theta) \\ \sin(\theta) & \cos(\theta) \end{pmatrix} \begin{pmatrix} s_{i,x}^t \\ s_{i,y}^t \end{pmatrix} + \begin{pmatrix} t_x \\ t_y \end{pmatrix}. \tag{7}$$

Given an initial pose estimate of the robot, the objective is to find $\Delta\zeta$ which minimizes the error

$$\sum_{i=1}^{n} \left[\bar{\varrho}_i^t - R(\mathbf{S}_i(\zeta + \Delta\zeta))\right]^2 \to 0. \tag{8}$$

The minimization of (6) can be performed by solving for $\Delta\zeta$ which yields the Gauss-Newton equation

$$\Delta\zeta = \sum_{i=1}^{n} \mathbf{H}^{-1} \left[\nabla R(\mathbf{S}_i(\zeta)) \frac{\partial \mathbf{S}_i(\zeta)}{\partial \zeta}\right]^T \left[\bar{\varrho}_i^t - R(\mathbf{S}_i(\zeta))\right],$$

where $\mathbf{H}$ corresponds to the hessian matrix which is calculated as

$$\mathbf{H} = \left[\nabla R(\mathbf{S}_i(\zeta)) \frac{\partial \mathbf{S}_i(\zeta)}{\partial \zeta}\right]^T \left[\nabla R(\mathbf{S}_i(\zeta)) \frac{\partial \mathbf{S}_i(\zeta)}{\partial \zeta}\right].$$

The term $\frac{\partial}{\partial \zeta}\mathbf{S}_i(\zeta)$ can be easily calculated from (7). In addition, the proposed extension of Hector SLAM takes advantage of the multi-resolution map as in [1] to escape local minima. An advantage of framing the pose estimation problem on gradient based methods is that the pose uncertainty can be directly computed from the inverse of the hessian matrix $\mathbf{H}$. This uncertainty can furthermore be used by SLAM back-ends [3], [5] to estimate the posterior distribution over the complete pose graph.

V. Experimental Evaluation

This section presents an qualitative and quantitative evaluation of the proposed approach. The first subsection focuses on highlighting the importance of the proposed LUT based model by showing the effect of ignoring the influence of extrinsic parameters whereas the second subsection presents an evaluation of the Hector SLAM extension.

A. Evaluation of the LUT-Based Model

To highlight the advantage of the proposed approach it is important to consider alternative models that ignore the influence of extrinsic parameters (r and α). The following subsection gives a brief description of the alternative models considered in this letter for comparison with the proposed approach.

1) Alternative Models: Given the extrinsic parameters (r and α) two different possibilities can be considered, firstly a model which ignores the effect of both r and α and directly uses the intensity increment I_{rec}. From here on in, this model is titled the *raw model*.

The second possibility is to model the influence of r, however systematically ignore the influence of α. In this letter the second model corrects the intensity increment I_{rec} based on $f(r)$ which is generated by fitting a polynomial

$$f(r) = \sum_{i=1}^{n+1} p_i r^{n+1-i},$$

to the intensity increment curve shown in Figure 1(a) and 1(b). Normalizing the intensity increment I_{rec} by the reference (white paper) polynomial curve $f(r)$ corrects the intensity based on r, however ignores the influence of α. This model is titled the *range model* for further reference.

2) Quantitative Evaluation: In this subsection a quantitative evaluation of the proposed approach is performed in comparison to the alternative models to highlight the importance of extrinsic parameter correction (r and α). In addition, it highlights the ability of the proposed approach to differentiate between surfaces of different reflectivities. To acquire data for this quantitative evaluation, *the laser scanner is mounted in a push-broom configuration (scanning vertically while the robot moves horizontally) thereby acquiring 3D models* of the environment as shown in Figure 4.

From the point cloud data, different samples (36000 point observations in total) were collected from 3 different surfaces marked in Figure 4(a). The points sampled from surface 1 correspond to different extrinsic parameters (r and α) whereas the sampled points of surface 2 and 3 exhibit significant variation in α only. Figure 3 shows the histograms after applying different models (raw, range and LUT based model) for the Hokuyo and SICK scanner. Considering the Hokuyo scanner first (see Figure 3(a), 3(b) and 3(c)), it can be seen in Figure 3(a) that the raw intensity histograms of surface 2 and 3 exhibit overlap whereas the histogram of surface 1 is multimodal. Applying the *range* model, it can be seen in Figure 3(b) that the histogram of surface 1 exhibits bimodality due to α variation whereas the histograms of surface 2 and 3 still overlap. Figure 3(c) shows the proposed approach (LUT based model correction) in which the histogram of surface 1 becomes unimodal whereas the overlap between the histograms of surface 2 and 3 has been effectively removed.

Figure 3(d), 3(e) and 3(f) show the same scenario in context of the SICK scanner. The first aspect to notice is that the variation in the intensity due to r and α is not as significant as in the case of the Hokuyo (see Figure 1). The histograms of surface 1 and 2 are separable even without extrinsic parameter correction whereas an overlap exists between the histograms of

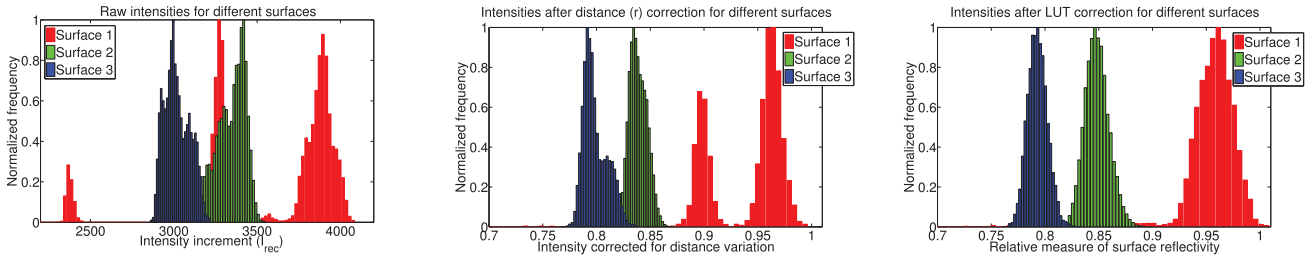

(a) Raw model for Hokuyo (b) Range model based correction for Hokuyo (c) LUT based model correction for Hokuyo

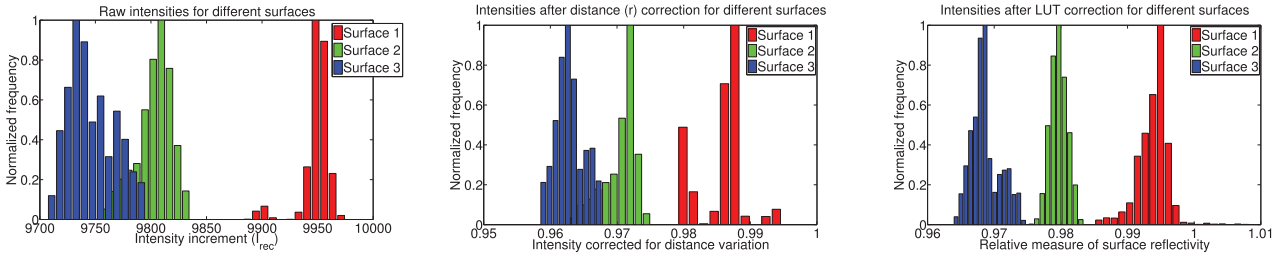

(d) Raw model for SICK (e) Range model based correction for SICK (f) LUT based model correction for SICK

Fig. 3. The histogram of intensities (with and without any correction) for different samples acquired from three different surfaces (see Figure 4(a)). The samples acquired from Surface 1 differ in r and α whereas the samples of surface 2 and 3 only vary in α. a,b) The histogram for the raw and the range model (see Section V-A1). The histograms corresponding to the raw and range correction model exhibit multimodality for surface 1 (due to r and α variation respectively) whereas surface 2 and 3 overlap. c) In contrast the proposed LUT based model is capable of identifying that these surfaces have different reflectivity characteristics. d,e) The histogram of intensities for the raw and range correction model for the SICK scanner. It can be seen that the histogram of surface 2 and 3 overlap. f) The LUT based model is capable removing the overlap between the histograms of surface 2 and 3 and makes all the histograms identifiable as surfaces of different reflectivity characteristics.

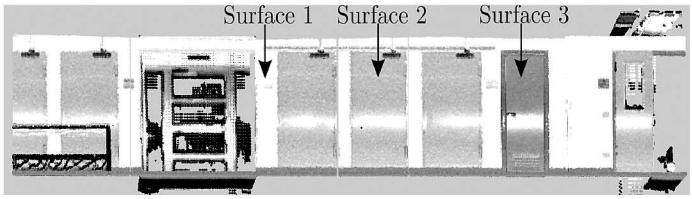

(a) Visualization of surface reflectivity characteristics in gray scale after the LUT based model correction for the Hokuyo scanner

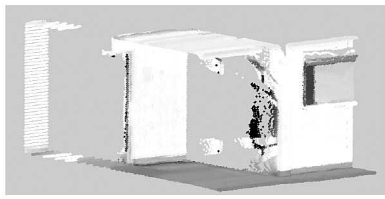

(b) Visualization of surface reflectivity characteristics in gray scale after the LUT based model correction for the SICK scanner

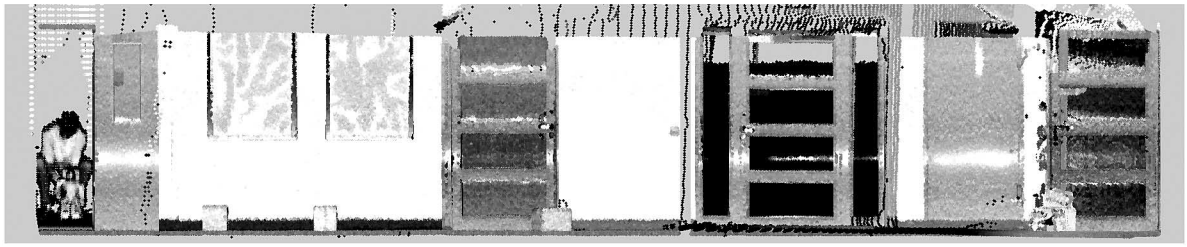

(c) Visualization of surface reflectivity characteristics for a corridor scene

Fig. 4. a-c) Visualization of surface reflectivity characteristics in gray scale image after the LUT based model correction with an additional linear scaling step to enhance contrast. A substantial region of the intensity point cloud shown in a) is also visible in the color image of Figure 5(b). It is important to highlight that the white horizontal region visible in a,c) across different surfaces is present due to specular reflection (in contrast to the standard diffuse reflection). This specular reflection occurs at a small angle of incidence for shiny and smooth surfaces as a significant amount of the emitted power is reflected back from the surface causing the receiver to register a maximum reading.

surface 2 and 3 due to variation in α. The *range* model shown in Figure 3(e) does not provide any significant advantage, however the *LUT* based model correction is capable of removing the overlap between the histograms of surface 2 and 3. *Hence, the evaluation of this section shows that extrinsic parameter correction is essential in context of identifying surfaces of different reflectivity characteristics.*

B. Evaluation of Hector SLAM (Front–End) Extension

This subsection evaluates the proposed Hector SLAM extension. To present a concise evaluation and avoid repetition of similar conclusions/figures this section presents the results using the Hokuyo scanner, however the conclusions are valid for the SICK scanner as well. Figure 5(a) shows the reflectivity map of the corridor at the Chair of Automatic

(a) Occupancy grid augmented with surface reflectivity characteristics

(b) Correspondence between reflectivity map and actual surface

Fig. 5. a) Occupancy grid augmented with surface reflectivity characteristics (using a HSV colormap) acquired by the proposed extension of Hector SLAM. The overall area composed of free and occupied regions is approximately 120 m^2 (ignoring unknown regions). b) A zoomed in section of the occupancy grid of Figure 5(a) highlighting the correspondences with the actual surface. *The laser scanner is mounted at a height of approximately 70 cm from the ground*. The corridor section visible in the color image is also observable in Figure 4(a).

(a) Hector SLAM

(b) Intensity based Hector SLAM

Fig. 6. A specific scenario highlighting the advantage of intensity based Hector SLAM over standard Hector SLAM. The field of view (FOV) of the scanner based on the minimum and maximum angle is $[-1.047\ 1.047]$ radians. The dimensions of the room are approximately 8.5 m $\times$ 5.5 m. a) Hector SLAM failed to create a consistent map as it could not find sufficient geometric features for pose estimation while turning at two different corners. b) Intensity based Hector SLAM succeeded in generating a consistent map as it additionally utilizes surface reflectivities for pose estimation.

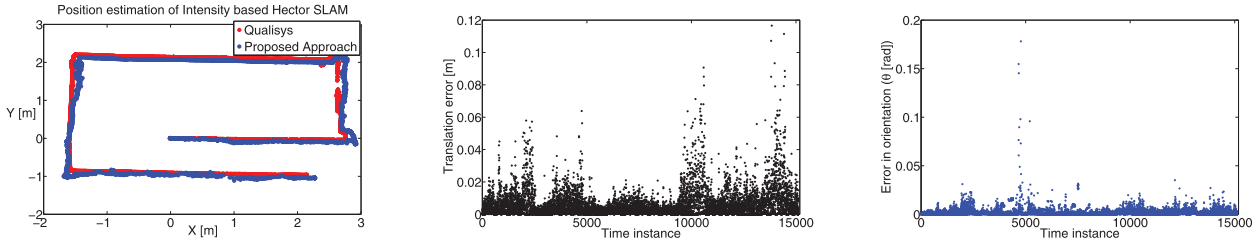

(a) Robot trajectory and groundtruth

(b) Translation error over time

(c) Orientation error over time

Fig. 7. a) Comparison of the trajectory estimated by the robot using the proposed extension of Hector SLAM with the ground truth (from the Qualisys MOCAP system). b,c) A plot of the translation and orientation errors [28].

Control Engineering (shown with a HSV colormap) whereas Figure 5(b) shows one specific section of the occupancy grid marked with arrows to highlight the correspondence with the actual surface. In addition, Figure 6(a) and Figure 6(b) highlight the advantage of intensity based Hector SLAM over standard Hector SLAM. In this specific scenario Hector SLAM failed to create a consistent metric map as it could not find sufficient geometric features for pose estimation while turning at two different corners. In contrast, intensity based Hector SLAM succeeded as it relied on surface reflectivity characteristics. In addition to the qualitative results in Figures 5 and 6, a quantitative evaluation of the proposed Hector SLAM extension is carried out using the MOCAP (motion capture) data acquired from the Qualisys system[4] which is capable of measuring the robot position with millimeter accuracy. Figure 7(a) shows the visualization of the ground truth trajectory (Qualisys system) as well as the robot positions obtained from the Hector SLAM extension. It is important to specify that qualisys motion capture system requires coverage (via external cameras) over the complete region where the robot has to be tracked, hence the evaluation of the motion could not be carried out in a large area. Figure 5(a) and 7(a) show that the proposed relative reflectivity measure can be used effectively to estimate the robot pose. In addition, a quantitative evaluation of the error for the proposed approach is performed using the metric defined in [28] as

$$\epsilon(\delta) = \frac{1}{N}\sum_{ij}(\delta_{ij} \ominus \delta^*_{ij})^2,$$

where δ_{ij} corresponds to the difference between consecutive robot poses at time index i, j and δ^*_{ij} corresponds to the

[4]http://www.qualisys.com/

ground truth variation in the pose. This δ_{ij} difference is split into the translation and the orientation error which is shown separately as a function of time in Figure 7(b) and 7(c) as in [28]. *The evaluation of this section highlights that the proposed approach is capable of estimating the robot pose accurately as well as acquiring a geometric model augmented with surface reflectivity characteristics*.

VI. Conclusion and Future Work

This letter discusses a *data-driven* approach to model laser intensities and identifies their role in the context of SLAM. An evaluation is carried out in indoor environments to highlight the effects of ignoring the influence of extrinsic parameters when acquiring surface reflectivity characteristics. The proposed mechanism for modeling laser intensities is tested and evaluated using two of the most commonly used scanners in the field of robotics. In addition, this letter presents a concrete example on how the proposed measure can be coupled with an extension of Hector SLAM to acquire a reflectivity map of the environment. The scan matching mechanism in the Hector SLAM extension is based on surface reflectivities and possess the capability of estimating the robot pose accurately. Furthermore, the experimental evaluation shows that surface reflectivities can be useful in cases when metric information is insufficient for pose estimation and consistent map generation.

Future work includes an evaluation of the relative reflectivity measure in outdoor urban environments as well as an assessment of its application in the domain of loop closure and global localization. It will also be worth looking into scenarios where the intensity based Hector SLAM approach can fail i.e. cases in which the normal vector estimation is inaccurate for a majority of the sensor observations due to low point density. In such cases it would be beneficial to integrate surface attributes (reflectivity/color) with metric information in the approach along the lines of [29], [30].

Acknowledgment

The authors would like to thank Thomas Wildgruber and Christoph Allig for the help in acquiring the intensity characteristics of the SICK and Hokuyo scanners. In addition, special thanks to Christoph Fröhlich, Markus Mettenleiter for the discussion about the Z+F scanner and Kai M. Wurm, Biruk A. Gebre for providing information about the undocumented mode of the SICK scanner. The authors would also like to thank the support of the TUM Institute for Advanced Study (IAS), Technische Universität München (TUM).

References

[1] S. Kohlbrecher, J. Meyer, O. von Stryk, and U. Klingauf, "A flexible and scalable slam system with full 3D motion estimation," in *Proc. IEEE Int. Symp. Safety Sec. Rescue Robot. (SSRR)*, Nov. 2011, pp. 155–160.

[2] G. Grisetti, C. Stachniss, and W. Burgard, "Improved techniques for grid mapping with Rao-Blackwellized particle filters," *IEEE Trans. Robot.*, vol. 23, no. 1, pp. 34–46, Feb. 2007.

[3] M. Kaess, A. Ranganathan, and F. Dellaert, "iSAM: Incremental smoothing and mapping," *IEEE Trans. Robot.*, vol. 24, no. 6, pp. 1365–1378, Dec. 2008.

[4] G. Grisetti, R. Kümmerle, C. Stachniss, and W. Burgard, "A tutorial on graph-based SLAM," *IEEE Intell. Transp. Syst. Mag.*, vol. 2, no. 4, pp. 31–43, Dec. 2010.

[5] M. Kaess, H. Johannsson, R. Roberts, V. Ila, J. J. Leonard, and F. Dellaert, "iSAM2: Incremental smoothing and mapping using the Bayes tree," *Int. J. Robot. Res.*, vol. 2, pp. 216–235, 2011.

[6] F. Dellaert, D. Fox, W. Burgard, and S. Thrun, "Monte Carlo localization for mobile robots," in *Proc. IEEE Int. Conf. Robot. Autom.*, 1999, vol. 2, pp. 1322–1328.

[7] P. Newman and K. Ho, "Slam-loop closing with visually salient features," in *Proc. IEEE Int. Conf. Robot. Autom.*, 2005, pp. 635–642.

[8] S. Khan and D. Wollherr, "IBuILD: Incremental bag of binary words for appearance based loop closure detection," in *Proc. IEEE Int. Conf. Robot. Autom. (ICRA)*, 2015, pp. 5441–5447.

[9] W. Fang, X. Huang, F. Zhang, and D. Li, "Intensity correction of terrestrial laser scanning data by estimating laser transmission function," *IEEE Trans. Geosci. Remote Sens.*, vol. 53, no. 2, pp. 942–951, Feb. 2015.

[10] R. B. Rusu, "Semantic 3D object maps for everyday manipulation in human living environments," *KI-Künstliche Intelligenz*, vol. 24, no. 4, pp. 345–348, 2010.

[11] J. Guivant, E. Nebot, and S. Baiker, "Autonomous navigation and map building using laser range sensors in outdoor applications," *J. Robot. Syst.*, vol. 17, no. 10, pp. 565–583, 2000.

[12] H. Yoshitaka, K. Hirohiko, O. Akihisa, and Y. Shin'ichi, "Mobile robot localization and mapping by scan matching using laser reflection intensity of the sokuiki sensor," in *Proc. IEEE 32nd Annu. Conf. Ind. Electron. (IECON)*, 2006, pp. 3018–3023.

[13] P. J. Besl and N. D. McKay, "Method for registration of 3-D shapes," in *Proc. Robot. DL Tentative*, 1992, pp. 586–606.

[14] A. Carballo, A. Ohya, and S. Yuta, "People detection using range and intensity data from multi-layered laser range finders," in *Proc. IEEE/RSJ Int. Conf. Intell. Robots Syst. (IROS)*, 2010, pp. 5849–5854.

[15] J. Levinson and S. Thrun, "Robust vehicle localization in urban environments using probabilistic maps," in *Proc. IEEE Int. Conf. Robot. Autom. (ICRA)*, 2010, pp. 4372–4378.

[16] C. McManus, P. Furgale, and T. D. Barfoot, "Towards appearance-based methods for lidar sensors," in *Proc. IEEE Int. Conf. Robot. Autom. (ICRA)*, 2011, pp. 1930–1935.

[17] K. M. Wurm, H. Kretzschmar, R. Kümmerle, C. Stachniss, and W. Burgard, "Identifying vegetation from laser data in structured outdoor environments," *Robot. Auton. Syst.*, vol. 62, no. 5, pp. 675–684, 2014.

[18] K. Fuerstenberg and K. Dietmayer, "Object tracking and classification for multiple active safety and comfort applications using a multilayer laser scanner," in *Proc. IEEE Intell. Veh. Symp.*, Jun. 2004, pp. 802–807.

[19] J. Hancock, M. Hebert, and C. Thorpe, "Laser intensity-based obstacle detection," in *Proc. IEEE/RSJ Int. Conf. Intell. Robots Syst.*, Oct. 1998, vol. 3, pp. 1541–1546.

[20] N. Pfeifer, P. Dorninger, A. Haring, and H. Fan, "Investigating terrestrial laser scanning intensity data: Quality and functional relations," *Proc. 8th Conf. Opt. 3-D Meas. Tech.*, Zürich, 2007, pp. 228–337.

[21] A. V. Jelalian, *Laser Radar Systems*. Norwood, MA, USA: Artech House, 1992.

[22] B. Gebre *et al.*, "Remotely operated and autonomous mapping system (roams)," in *Proc. IEEE Int. Conf. Technol. Pract. Robot Appl.*, 2009, pp. 173–178.

[23] B. Höfle and N. Pfeifer, "Correction of laser scanning intensity data: Data and model-driven approaches," *ISPRS J. Photogramm. Remote Sens.*, vol. 62, no. 6, pp. 415–433, 2007.

[24] R. Blaskow and D. Schneider, "Analysis and correction of the dependency between laser scanner intensity values and range," *Int. Arch. Photogramm. Remote Sens. Spatial Inf. Sci.*, vol. 25, pp. 107–112, 2014.

[25] A. Hornung, K. M. Wurm, M. Bennewitz, C. Stachniss, and W. Burgard, "OctoMap: An efficient probabilistic 3D mapping framework based on octrees," *Auton. Robots*, vol. 34, pp. 1–18, 2013.

[26] S. Khan, A. Dometios, C. Verginis, C. Tzafestas, D. Wollherr, and M. Buss, "Rmap: A rectangular cuboid approximation framework for 3D environment mapping," *Auton. Robots*, vol. 37, pp. 1–17, 2014

[27] S. Khan, D. Wollherr, and M. Buss, "Adaptive rectangular cuboids for 3D mapping," in *Proc. IEEE Int. Conf. Robot. Autom. (ICRA)*, 2015, pp. 2132–2139.

[28] W. Burgard *et al.*, "A comparison of SLAM algorithms based on a graph of relations," in *Proc. IEEE Int. Conf. Intell. Robots Syst.*, 2009, pp. 2089–2095.

[29] A. E. Johnson and S. B. Kang, "Registration and integration of textured 3D data," *Image Vis. Comput.*, vol. 17, no. 2, pp. 135–147, 1999.

[30] B. Huhle, M. Magnusson, W. Straßer, and A. J. Lilienthal, "Registration of colored 3D point clouds with a kernel-based extension to the normal distributions transform," in *Proc. IEEE Int. Conf. Robot. Autom. (ICRA)*, 2008, pp. 4025–4030.